

# Design and construction progress of BRIF<sup>\*</sup>

ZHANG Tian-Jue(张天爵)<sup>1)</sup> GUAN Xia-Ling(关遐龄) CUI Bao-Qun(崔保群)

China Institute of Atomic Energy, Beijing 102413, China

**Abstract** A new RIB project, the Beijing Radioactive Ion-beam Facility (BRIF), has been running at CIAE since 2004. In this project, a 100 MeV H<sup>-</sup> cyclotron, CYCIAE-100, is selected as the driving accelerator providing a 75–100 MeV, 200–500  $\mu$ A proton beam. An ISOL system employs two stage separators to reach the mass resolution of 20000. Its RIB beam will be injected into the existing Tandem and a superconducting booster installed down stream of the Tandem will increase the energy by 2 MeV/q. The progress of BRIF, giving special emphasis to CYCIAE-100, will be introduced in this paper.

**Key words** cyclotron, main magnet, RF cavity, ISOL, QWR, superconducting cavity

**PACS** 29.20.-c

## 1 Introduction

For production of an intense proton and radioactive ion beam (RIB) used in fundamental and applied research, e.g., neutron physics, nuclear structure, material and life sciences and medical isotope production, a new RIB facility, Beijing Radioactive Ion-beam Facility (BRIF) has been running at CIAE since 2004 [1]. In this project, a 100 MeV H<sup>-</sup> cyclotron, normally referred to as CYCIAE-100 [2], is selected as the driving accelerator aiming to provide simultaneously a 75 MeV–100 MeV, 200  $\mu$ A – 500  $\mu$ A proton beam for 7 beam lines, generate neutrons for the 15 m and 30 m transport lines, and generate an

RIB for low energy applications and injection into the Tandem. The basic design and construction progress of BRIF will be depicted, including CYCIAE-100, ISOL, and the SCB (superconducting booster). A sketch of BRIF is shown in Fig. 1. The new building for CYCIAE-100 and ISOL is to the west of the existing Tandem building and both are combined together. The SCB will be installed in the Tandem Hall.

## 2 General designs of CYCIAE-100 and basic beam dynamics

The adoption of a compact, deep valley structure for CYCIAE-100 makes it possible to provide strong vertical focusing to meet the requirement of intensive beam acceleration. It uses 4 straight sectors instead of spiral sectors, which are used basically for the AVF cyclotron with an energy higher than 70 MeV. The H<sup>-</sup> beam is extracted by carbon foil stripping with very small beam loss from calculation and testing. To reduce the beam loss induced by the Lorentz stripping, the hill field at the outer region is less than 1.4 T to ensure the beam loss is less than 0.3%. Vacuum dissociation is another reason to induce beam loss in this H<sup>-</sup> machine, which requires the vacuum in the main tank to be better than  $5 \times 10^{-6}$  Pa level on average. For the RF system, it adopts a double Dee structure and fourth harmonics. Two resonant

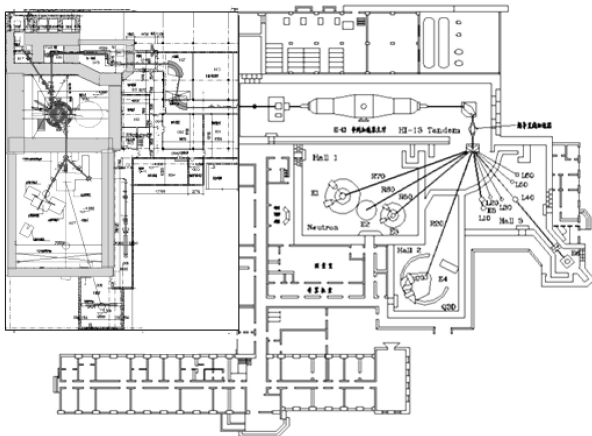


Fig. 1. Sketch map of BRIF.

Received 5 February 2009

\* Supported by NSFC (10125518)

1) E-mail: tjzhang@ciae.ac.cn

©2009 Chinese Physical Society and the Institute of High Energy Physics of the Chinese Academy of Sciences and the Institute of Modern Physics of the Chinese Academy of Sciences and IOP Publishing Ltd

cavities of half wave length are completely installed and fixed in the valley of the magnet. The machine structure and most of the sub-systems are shown in Fig. 2.

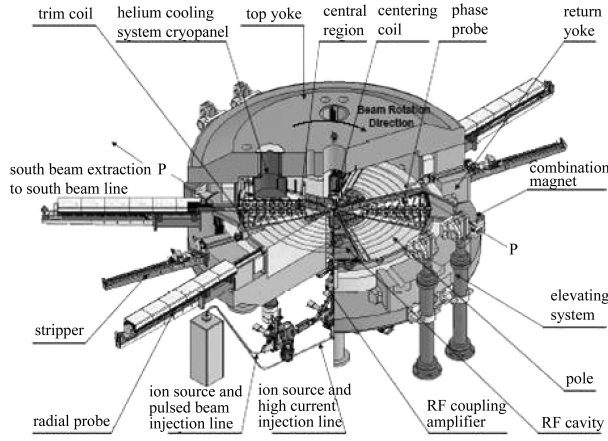


Fig. 2. The overall structure of CYCIAE-100.

After a static equilibrium orbit study for tune,

phase shift and stable area etc., it is concluded that the vertical tune  $\nu_z$  for this compact cyclotron is higher than 0.5 at most of the acceleration region and up to 0.7. This is of advantage for upgrading the beam intensity later on. Also, the transverse acceptance is big enough for high current  $H^-$  beam injection.

The accelerating beam dynamics is also investigated in detail. The beam matching from 0.1 MeV to final energy has been done step by step by single particle tracking. The tracking of about 20 thousand particles by COMA, a TRIUMF code modified by CIAE [3], is started from a static ellipsoid with 0.3 cm displacement, centered at the AEO (accelerated equilibrium orbit) at 5 MeV, and with a RF phase band of  $40^\circ$ . The simulation results of radial phase space matching are shown in Fig. 3, from which it can be noticed that the radial phase is compressed obviously due to the increase of accelerating voltage (Fig. 7). That would improve the extracted beam quality and decrease the  $H^-$  beam losses by EM stripping at the higher energy region.

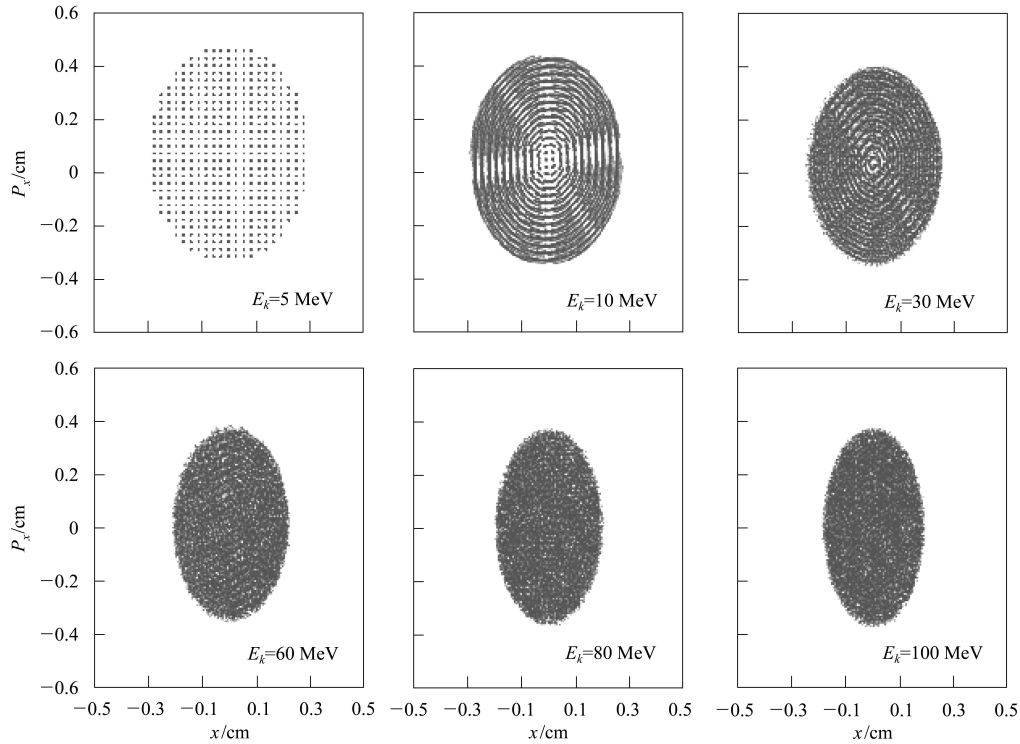


Fig. 3. Matching of radial phase space, 5 MeV to 100 MeV.

### 3 Main magnet

#### 3.1 The structure parameters

Based on the consideration that the beam intensity limitation is increased with the enhancement of

vertical focusing and the power consumption of the main coils is reduced by taking a compact structure, the hill gap between the poles should be small enough. However, taking into account the installation of RF liner, centering coils, and diagnostics devices the hill

gap should be sufficiently large. After comparing several solutions, a relatively comprehensive option [4] is adopted, i.e., 6 cm at the center, gradually changing to 5 cm at the external region.

After adjusting the pole shape, central plug, hill and valley gap, etc. the main parameters of the mag-

net are obtained (Table 1). The result from numerical simulation shows that the isochronous is good for ensuring the integral phase shift is within  $\pm 10^\circ$  and that  $\nu_z$  increases and successfully avoids all the harmful resonance, e.g. the Walkinshaw at high energy [2].

Table 1. Main parameters of magnet.

number of sector	4	radius of poles	2000 mm
outer diameter	6160 mm	angle of poles	47°
dimension height	2820 mm	height of poles	765 mm
hill gap	50–60 mm	thickness of top/bottom yoke	775 mm

### 3.2 Imperfection simulation

The simulation results from the accelerating beam dynamics study show us that the magnetic field for CYCIAE-100 should satisfy the following conditions: the 1st harmonic is around 2 Gauss, the 2nd harmonic is less than 40 Gauss, and the gradient of the 2nd harmonic is less than 8 Gauss/cm.

#### 3.2.1 Defects from the steel production process

It is inevitable that some factors will result in the intrinsic asymmetry of the magnetic field, such as segregation, contraction cavity, shrinkage porosity, dross inclusion, etc., which would come up in the process of casting and forging. The defects will impose an influence on the uniformity of the magnetic field.

The magnet is divided into three zones (Zone 1: from the pole surface to a depth of 100 mm, Zone 2: other portion of the pole, Zone 3: all the yokes). When we calculate the effect of imperfections on the magnetic field, all imperfections are assumed as ellipsoid shape. The 3D FEM results give the tolerable dimensions of defects for ultrasonic flaw detection (Table 2).

Table 2. Tolerable defect of each zone in the magnet.

	Zone 1	Zone 2	Zone 3
in an area of 200 mm×200 mm, less than 5 equivalent diameter “ $\Phi$ ”	$\Phi 2$ mm	$\Phi 4$ mm	$\Phi 8$ mm
equivalent diameter “ $\Phi$ ”	$\Phi 3$ mm	$\Phi 6$ mm	$\Phi 12$ mm

The diversity of the chemical composition, and then that of the permeability between poles, and between the yokes will produce the 1st harmonic in median plane. In simulation, the BH curve of one pole is selected as 99% and 95% of the other 3, and the maximum amplitude of the 1st and 2nd harmonic is calculated by FFT based on the calculated field. Similar approaches are used for the yoke simulation. The

technical requirements of chemical composition are accordingly estimated and specified. The uniformity of chemical composition is required to be:

1) For the pole (8 pc), central plug (2 pc), shimming bar (16pc+24pc spare),  $C < 0.050\%$ , and difference between parts DC  $< 0.01\%–0.02\%$ .

2) For the top/bottom yokes (2 pc), return yokes (4 pc),  $C < 0.13\%$ , and the difference between parts at the same locations) DC  $< 0.03\%–0.04\%$ .

#### 3.2.2 Stress and deformation simulation

To reduce the hill gap deformation, the top/bottom yokes are optimized to an uneven-height structure (different height along the radius). The upper part of the magnet, including the top yoke and four sectors, weighs 170 t in total. The electromagnetic force is 420 t between the sectors, and the atmospheric pressure on the top yokes is estimated as about 120 t. When the even-height structure is chosen in the stress field simulation, the deformation is 299  $\mu\text{m}$  at the radius of 25 cm. To properly arrange the magnetic flux and to keep the weight of the top/bottom yokes unchanged as compared with the original, even-height structure, the uneven-height structure of the yokes has been optimized to reduce the deformation. The designed result is shown in Fig. 4, while the deformation is reduced to 210  $\mu\text{m}$ , by about 35%. It is of even more importance that

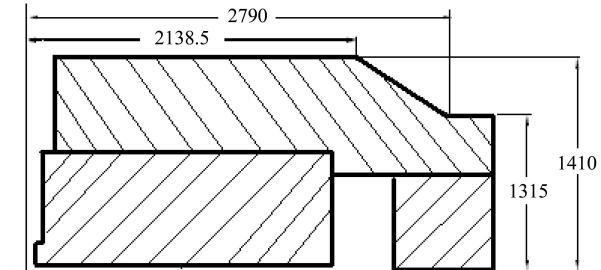


Fig. 4. The top/bottom yokes of uneven height.

relative deformation caused by vacuum pressure is reduced by about 41% since field mapping is in an atmospheric environment, while the cyclotron operates in a vacuum. Though the deformation is reduced obviously, the vacuum compensation remains crucial during the mapping.

### 3.3 Magnet construction

Before proceeding with the contract for steel, we decided that the poles, central plugs and shimming bars adopted forged pure iron; the yokes adopted GB 8# steel in the light of China's standard and casting piece could be considered for use.

The steel for the poles was contracted from Industeel in Lyon, France and was shipped to CIAE in April 2008. The casting piece and rough machining were contracted from CITIC Heavy Machinery Co. Ltd. in Luoyang, China and were finished by December 2008. Fig. 5 shows the main part of the magnet under machining. The carbon segregation at the same circle and same height of the yokes is within 0.03%. Recently, the rough machining of the top/bottom yokes and return yokes has been finished.



Fig. 5. The top/bottom yokes under machining.

## 4 RF cavity design

### 4.1 Cavity design with double stems

Two RF cavities are designed to install into the two opposite valleys with a resonant frequency of about 44.45 MHz. It is also expected from the beam dynamics that the Dee voltage should be about 60 kV at the central region and about 120 kV at the large radius region. The cavities are RF shielded at the machine center and driven by two 100 kW amplifiers independently [5]. The double-stem structure (Fig. 6 and Table 3) is adopted to control the voltage distribution and adjust the frequency by the position and diameter of the stems and the Dee shape in practice, from which we obtain the required resonant frequency and the unloaded  $Q$  value of approximately 10300. The scaled voltage, integrated from the calcu-

lated E-field, is increased as shown in Fig. 7. A 1:1 scale wooden model was fabricated to measure the frequency, matching and accelerating voltage. The error, compared with the design value, is about 5% for the Dee voltage (Fig. 7) and 1% for the frequency, respectively.

Table 3. Principal structural parameters of the cavity.

outer conductor		inner conductor	
height	1.26m	Stem1	6.4 cm
		Stem2	7 cm
outer radius	1.98 m	length of the Dee plate	1.86 m
angle	36.6°	angle of the Dee plate	34.4°

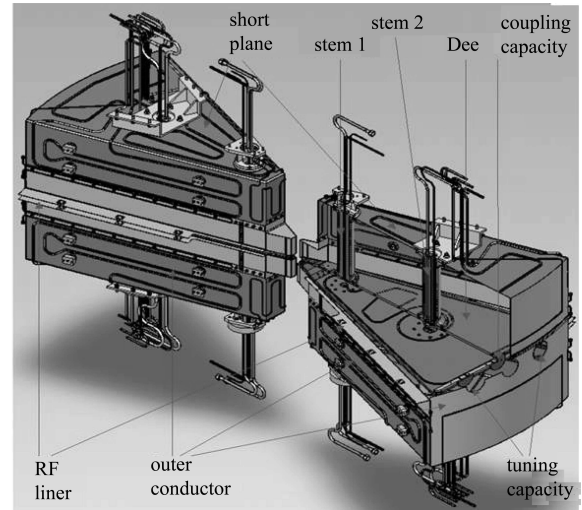


Fig. 6. The structure of the double-stem cavity.

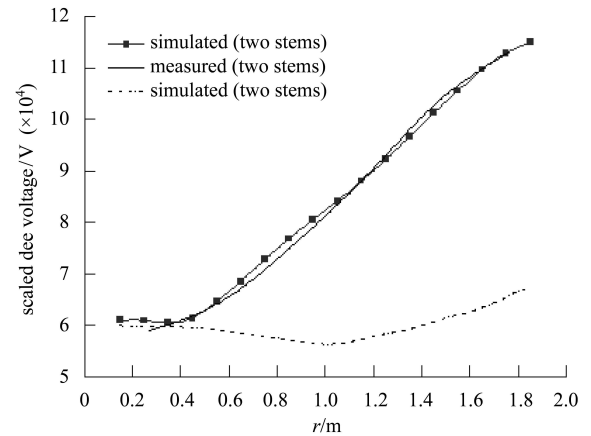


Fig. 7. Dee voltage, simulation and measurement.

### 4.2 Thermal analysis

The water cooling of the RF cavity has to be well arranged to limit the temperature rise and keep the operation stability so that the RF frequency will remain stable within the range of fine tuning by

LLRF control on line. From the numerical simulation,  $\sim 28.1$  kW power will be dissipated on each cavity ( $Q = 10300$ ). However, taking into consideration the practical fabrication, the actual  $Q$  value could be

estimated as  $\sim 6000$ . Therefore, the dissipated power per cavity will be  $\sim 48.2$  kW. Table 4 shows the power loss on Dee, inner stem, outer stem, wall, short plate, capacitance and RF liner at different  $Q$  values.

Table 4. The distribution of power loss on each RF cavity.

$Q$ value	total power loss/kW	power distribution/W						
		dee	inner stem	outer stem	wall	short plate	capacitance	RF liner
$Q=10300$	28.1	6280	7920	5840	3246.8	1408	76	3324
$Q=6000$	48.2	10800	13600	10020	5575	2417	130	5706

A helical water cooling tube is used inside both of the stems. On the RF liner and all the cavity wall, water cooling tubes are welded on their surface. In the Dee, the water cooling tubes are embedded inside the Dee plate. The results from numerical thermal analysis show that the maximum temperature rise of the Dee is  $12.6^\circ\text{C}$  and  $18.3^\circ\text{C}$ , the inner stem is  $3.2^\circ\text{C}$  and  $5.6^\circ\text{C}$ , while the  $Q$  value is 10300 and 6000 respectively.

#### 4.3 The analysis of tolerance for the RF cavity

The fabrication tolerance will disturb the radial and vertical motion of the beam, and the deformation of the Dees caused by gravity will lead to axial misalignment of the Dees and then induce the build-up of coherent axial oscillations. These are investigated in detail and published elsewhere [6].

#### 4.4 The RF system construction

The RF cavities, two 100 kW amplifiers and their coaxial transmission lines are under construction and will be ready for testing by the end of 2009. The cavities under construction are given in Fig. 8. Close loop tests for 1<sup>st</sup> prototype boards for low level RF control have been successfully conducted in July 2006. The phase stability is better than  $0.3^\circ$ , and the amplitude stability is better than 2%.



Fig. 8. The 44.45 MHz RF cavity under construction.

## 5 Injection and extraction

### 5.1 The ion source test stand

To optimize the injection efficiency from the source to the cyclotron central region, a cusp source has been being developed at CIAE since 2003. A beam of more than 10 mA with a measured emittance of  $0.65 \pi \text{ mm mrad}$  is obtained at 28 kV from an extraction hole of 11 mm in diameter (Fig. 9).

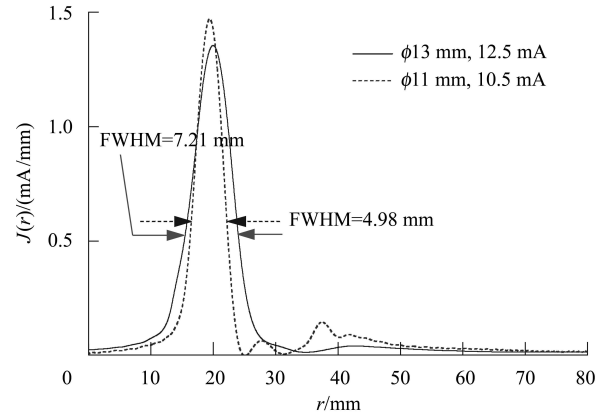


Fig. 9. The beam profiles with different extraction apertures.

Recently, a new test stand for  $\text{H}^-$  source has been developed since the old one is used for a 10 MeV CRM cyclotron. A  $\sim 15$  mA DC  $\text{H}^-$  beam was extracted from the initial test. The measured emittance is  $0.45 \pi \text{ mm-mrad}$  while the extracted beam is 11 mA.

### 5.2 The axial injection line

The extracted beam intensity for CYCIAE-100 is required to reach  $200 \mu\text{A}$ , and it is planned to provide a pulsed beam as well. In order to get a high average beam intensity and to be capable of providing the pulsed beam, two beam lines for the axial injection are considered, corresponding to Line 1# and Line 2# respectively [7]. Line 1# takes advantage of



a switching magnet are used right after each combination magnet to focus and to distribute the proton beam in different lines (Fig. 1). The construction design and the test of the key parts, e.g. the  $10^{-8}$  Torr air lock system for the 12 carbon foil exchanger are finished.

For the beam line design and optics matching, the matrix from the stripping point to the combination magnet should not be ignored since the fringe field effect is strong and the dispersion is usually high in the compact machine. The orbit tracking of extracted proton beams has been studied with CIAE's code CYCTR. The first order transfer matrix is obtained from GOBLIN [10], which was modified by CIAE for the matrix calculation [11]. One of the results is:

$$M = \begin{pmatrix} 0.992 & 0.206 & 0 & 0 & 0 & 0.656 \\ -0.431 & 0.918 & 0 & 0 & 0 & 4.080 \\ 0 & 0 & 0.503 & 0.192 & 0 & 0 \\ 0 & 0 & -2.619 & 0.988 & 0 & 0 \\ -0.433 & -0.024 & 0 & 0 & 1 & 1.607 \\ 0 & 0 & 0 & 0 & 0 & 1 \end{pmatrix}.$$

The dispersions during beam extraction for two locations of the combination magnet are investigated and compared with various energies from 75 MeV to 100 MeV. The location (2.75 m,  $100^\circ$ ) is determined for the design and then all the beam lines are matched.

## 6 Other aspects of CYCIAE-100

For the  $10^{-6}$  Pa vacuum system, the design for the cryopanel is finished and the refrigerator selection has been carried out. To verify the design, a plug-in cryopump had been designed. It consists of two cryopanels, a baffle, a half-opened shield, and two GM refrigerators (CGR411,CVI) with a power of 83 W at 80 K and 7.5 W at 20 K. Its designed pumping speed is 15000 l/s. The test system employs the flux method to test pumping speed, cool-down time, ultimate pressure, temperature distribution on cryopanel. The construction of the plug-in cryopump is finished.

Work on the beam diagnostics, dose monitoring and safety interlock, including network-based signal acquisition, DCCT development, double wire scanner, emittance scanners and measuring for neutrons at a wider energy range have been finished as well.

## 7 The ISOL system

One of the 7 proton beam lines of CYCIAE-100, directly north of the machine, is for the ISOL system to generate more than 120 species of RIB with energies from 100 keV to 17 MeV/q. The system consists of a few sets of target-source modules and two stages of mass separators to reach a resolution up to 20000 (Fig. 13).

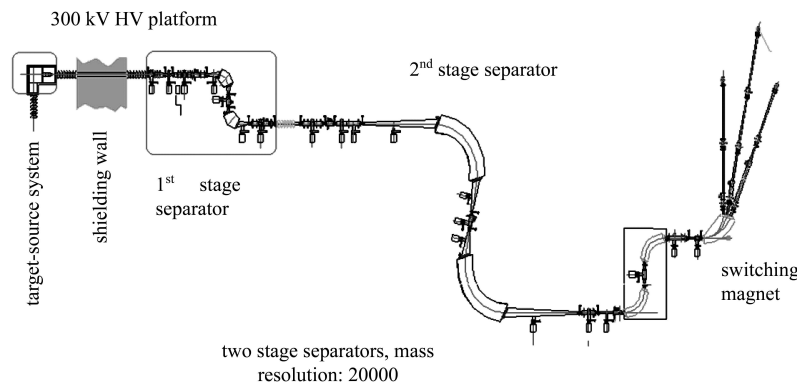


Fig. 13. The configuration of the ISOL system.

The work on the ISOL system has been well carried out and by now all the design schemes have been determined. Relevant experiments are being actively conducted and in smooth progress, providing a favorable environment for the construction design. Orders have been placed for all the major devices.

The processing chamber of the source-target is

very important because of the high dose and its close relationship with civil engineering. So far the technical specifications have been determined and the fabrication chamber was started at the end of 2007.

The design of the seven magnets used in the ISOL system (4 for the two stage separators) is finished. It is ready for bidding invitations. To eliminate the

aberration from magnets, the 3rd order surface coils have been tested. The measurement data are well consistent with design. The problems found from the test, e.g. higher temperature of the circuit board, non-zero field in the center will be investigated [12].

The field distribution of the electrostatic lens has been calculated and its mechanical design is being carried out. The technical specifications of various magnets, lenses and steering power supplies (about 150 sets) have been finished. The two high voltage power supplies with high stability and low ripple, 300 kV and 50 kV respectively, have been loaded.

Several tests are in progress, including the diagnostics for low beam intensity down to  $10^6 \text{ s}^{-1}$  and HV conduits through the shielding walls for high radiation environments, etc.

The 150 kV injector of the existing Tandem has been upgraded to 300 kV. The new injector system (Fig. 14) includes two beam lines. One is the high voltage platform beam line to match the superconducting booster. The other is a high resolution achromatic beam line for AMS. The experimental results show that the mass resolution is better than 480 [13].

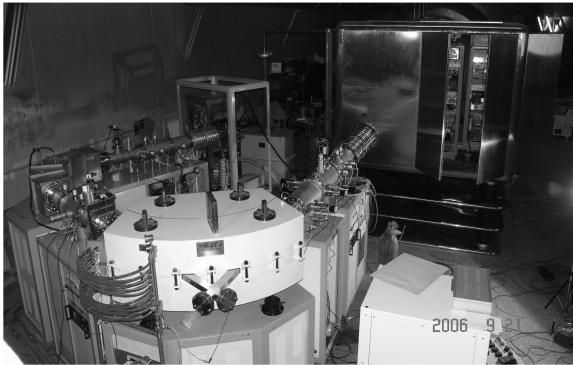


Fig. 14. The new injector for HI-13 Tandem.

## 8 The Super Conducting Booster (SCB)

Four niobium-copper QWR cavities will be put into one cryostat, which will be installed downstream of the existing Tandem to provide an energy gain of 2 MeV/q for  $\beta=0.118$  ions [14]. The layout of SCB installed between the Tandem and the switching magnet is shown in Fig. 15. The designed primary parameters are given as follows:

- 1) Temperature 4.2 K;
- 2) Frequency 150.4 MHz;
- 3) Accelerated gradient 3.5 MV/m;
- 4) The power consumption of the cryogenic system is 50 W.

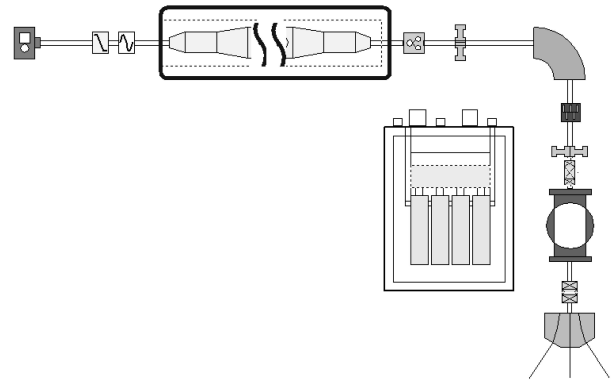


Fig. 15. The layout of the superconducting booster between Tandem and the switching magnet.

### 8.1 Copper base of the SC cavity

The machining procedure for the copper base of the QWR cavity without welding has passed the verification and progresses steadily in processing.

### 8.2 Niobium sputtering of the SC cavity

A laboratory for niobium sputtering for the QWR cavity is being rebuilt. The design for a high purging, high pressure water wash and water cooling cycle has been finished. Contracts for the clean room, electropolishing devices used for post processing of the QWR cavity and super high pressure water cleaning devices have been signed.

The contract for the technological development of high vacuum sputtering of the QWR cavity has been signed, and the machining has been finished. Related tests have been accomplished in the factory, and the take-over procedure will be scheduled soon.

### 8.3 Cryostat

The cryostat is composed of a vacuum container, a heat insulation shell, a liquid helium vessel and a support structure. The construction of the cryostat



Fig. 16. The cryostat for the QWR cavity.

has been finished (Fig. 16), and related liquid helium and vacuum experiments have been conducted. At present the setup service before the acceptance is being arranged.

#### 8.4 Low energy beam pulsing system

A low energy beam pulsing system is used to match the time-acceptance of the superconducting booster. A double drift buncher is designed with variable frequencies around 6 MHz and 12 MHz. A traveling wave chopper is installed before the buncher. At present, some special components are being developed.

The operating frequency of the booster is 150.4 MHz and the fundamental frequency of bunching is 6 MHz. Independent phase control is adopted in each loop. Now the TWC driver, the resonator

controller and the low noise amplifier are under test.

## 9 Conclusion and prospects

The design and construction of BRIF is being implemented. The construction of the major parts for CYCIAE-100, including the magnet and coils, the RF cavities and amplifiers, the  $H^-$  source, the vacuum, etc. is showing smooth progress. The development of the ISOL and SCB systems are spread in their entirety as well. It is expected that a revised feasibility report will be approved at the beginning of 2009, following which the building construction will be started. It is planned to obtain the first proton beam from CYCIAE-100 by the end of 2012 and the RIB will be provided in 2013.

## References

- 1 ZHANG T et al. Proc. of the 3rd Asia Particle Accelerator Conference, Korea, 2004, 267
- 2 ZHANG T et al. Proc. of 18<sup>th</sup> Inter. Conf. on Cyclotrons and Their Applications (Invited), Italy, 2007, 33
- 3 BI Y et al. Nuclear Instruments and Methods in Physics Research A, 2008, **597**(2-3): 149–152
- 4 ZHANG T et al. Nuclear Instruments and Methods in Physics Research B, 2007, **261**(1-2): 25–30
- 5 WANG X et al. CIAE Internal Report, BRIF-C-B03-01-SM, 2005
- 6 BI Y et al. Proc. of 18<sup>th</sup> Inter. Conf. on Cyclotrons and Their Applications, Italy, 2007, 458
- 7 YAO H et al. Rev. of Sci. Instrum., 2008, **79**(2): 708–710
- 8 ZHANG T et al. Atomic Energy Science and Technology, 1996, **30**(5): 399–404 (in Chinese)
- 9 Milton B F. TRIUMF design note, TRI-DN-89-19
- 10 Milton B F. TRIUMF design note, TRI-CD-90-01
- 11 WEI S et al. Nuclear Instruments and Methods in Physics Research B, 2008, **266**: 4697–4701
- 12 CUI B et al. Annual Report of CIAE, 2007, 78
- 13 BAO Y et al. Annual Report of CIAE, 2006, 54
- 14 ZHOU L et al. Annual Report of CIAE, 2007, 77